IOSUD - Universitatea Politehnica Timişoara
Şcoala Doctorală de Studii Inginereşti

Analysis of non-simmetries caused by faults in three-phase electrical installations

Ph.D. Thesis – Summary

for achieving the scientific title of Ph.D. at
University Politehnica Timisoara
in the doctoral field of Electrical Engineering

author Eng. Marian-Claudiu ŞOLEA
scientific coordinator Prof.Ph.D.Eng. Dumitru TOADER

July 2024

Table of contents

1. INTRODUCTION

Power delivery at medium voltage level over an ever-expanding electrical grid is more prone to faults than at other higher voltage level. The most common fault type in these electrical networks is the single line-to-ground fault. It is therefore necessary to design protection schemes that ensure a fast and selective detection of such faults. A reliable operation of the protective relays depends on both the accurate analytical computation and numerical modelling of the single line-to-ground fault current. This thesis tackles key issues of long-term scenario planning, namely the influence of the medium voltage distribution network parameters, such as the initial phase of the faulted line, the insulation state, the grounding method, and the Petersen coil resistance, provided that the network has resonant grounding, respectively, on the fault current and on the medium voltage busbars zero-sequence voltage based on which the protective relays make a discriminatory decision when such a fault occurs. The purpose of this endeavour is to emphasise that the setting of these relays must be reviewed periodically and updated according to the latest parameters values. This thesis is organised as follows: this first introductory chapter assesses the state-of-the-art regarding the single line-to-ground detection; a second chapter highlighting the analytical considerations for modelling of the medium voltage distribution network; a third chapter introducing the numerical model for the electrical network; a forth chapter analysing the influence of the upper mentioned parameters on the transient regime caused by a single line-to-ground fault; and a fifth chapter with concluding comments.

The main objectives of the doctoral thesis are:

- Evaluating the accuracy of the available analytical model used for the zero-sequence voltage and current computation for different grounding methods – isolated neutral, resistor grounded neutral and resonant grounding, respectively.
- Analysis of the influence of the network insulation electrical resistance on the zero-sequence voltage and current for different grounding methods – isolated neutral, resistor grounded neutral and resonant grounding, respectively.
- Analysis of the influence of the Petersen coil electrical resistance on the zero-sequence voltage and current for a resonant grounding network operating at resonance, overcompensation and undercompesantion, respectively.
- Analysis of the influence of the voltage initial phase at fault inception time on the transient component of the zero-sequence voltage and current for different grounding methods – isolated neutral, resistor grounded neutral and resonant grounding, respectively.
- Analysis of the influence of the network insulation electrical resistance on the transient component of the zero-sequence voltage and current for different grounding methods – isolated neutral, resistor grounded neutral and resonant grounding, respectively.
- Analysis of the influence of the Petersen coil electrical resistance on the transient component of the zero-sequence voltage and current for a resonant grounding network operating at resonance, overcompensation and undercompesantion, respectively.

2. ANALYSIS OF NON-SIMMETRIES CAUSED BY FAULTS IN THREE-PHASE ELECTRICAL INSTALLATIONS

The single line-to-ground faults [1], [2], [3], [4], [5] account for 70 to 90% of the total number of faults [6], [7], [8]. When they occur [9], [10], [11], both the three phase currents and the phase voltages do not summate to zero anymore. Numerical algorithms based on these assumptions are already implemented in protective relays for a fast and selective detection of such a fault [12], [13], [14], [15], [16], [17]. For a relay to be capable of making a discriminatory decision based on the zero-sequence components values, it is necessary do develop computational models that resemble the contingencies present in distribution networks during faults as accurate as possible. Mathematical models, analytical or numerical, are used to calculate the voltages and the currents flowing through the medium voltage electrical network during a single line-to-ground fault. Numerical models used to analyse this type of fault in medium voltage

distribution network with different grounding methods have been implemented in PSpice [6], [18], [19], [20], [21], [22], [23] and in the MATLAB programming environment [24].

The network from Fig. 1 has the neutral physical point grounded via an arc-suppression coil, the grounding method used for medium voltage networks with total capacitive current exceeding 10 amps. The role of the Petersen coil is to compensate this capacitive current.

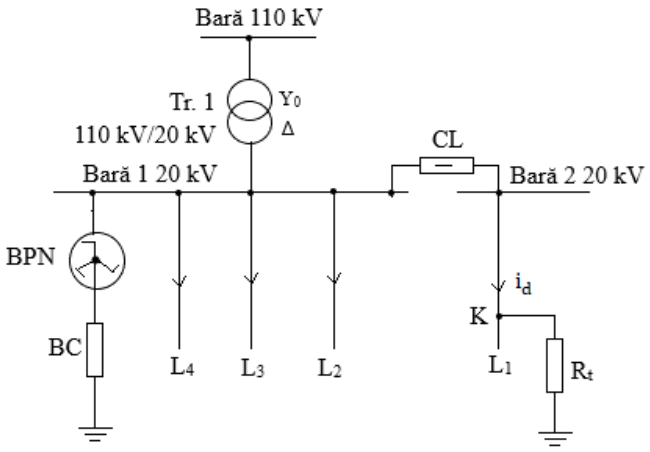

Fig. 1. Single line diagram of the substation and the medium voltage electrical network

The following notation conventions are used: HV for high voltage (the power system considered of infinite power) and MV for the medium voltage; Tr. 1 – three-phase transformer with the primary windings (high voltage) in wye connection with ground (Y_0) and the secondary windings (medium voltage) connected in delta (Δ); BPN – zig-zag coil (Z_0) used to create the network neutral physical point; BC – the Petersen coil used to ground the network neutral physical point, with the following parameters: resistance R_{BC} and inductance L_{BC}; R_t – the fault resistance; L_1, L_2, ..., L_4 – MV lines; K – fault location. The total phase-to-earth capacitance of the medium voltage network is the sum of the phase-to-earth capacitances of each medium voltage line (Fig. 1). The equivalent electrical resistance corresponding to the active power losses in the insulation of all medium voltage lines is expressed as a function of the equivalent electrical resistances corresponding to active power losses in each line. For an accurate representation of the real network, the equivalent electrical resistance that models the insulation imperfection is connected in parallel with the phase-to-earth capacitance. The total capacitive current of the medium voltage network contains both an active component and a reactive component. The phase angle difference between the total current and reactive component, denoted as δ, represents the insulation loss angle [25], [26]. If the active component of the total capacitive current is greater than 10 A, the Petersen coil no longer ensures the extinguishing of the electric arc when the current passes through the zero value, which is why it is necessary to disconnect the line from the source for eliminate the fault.

The method of symmetrical components is widely used to analytically determine currents and voltages during unsymmetrical short circuits [27], [28]. The zero-sequence equivalent electrical circuit of the medium voltage network considering also the resistance R_{BC} of the real Petersen coil is presented in Fig. 2, where the following notation conventions are used: X^0_{BPN}, R_{BPN} – the reactance and the electrical resistance of the zig-zag coil BPN; R_{BC}, L – the electrical resistance and the inductance of the Petersen coil; R_{iz} – the equivalent electrical resistance corresponding to active power losses in the insulation of the medium voltage network, and X^0_C – the capacitive reactance of the medium voltage electrical network. The value of the inductance L of the Petersen coil depends on the total capacitive reactance of the medium voltage network X^0_C, the reactance X_{BPN}, the resistance R_{BPN} of the zig-zag coil and the resistance R_{BC} of the Petersen coil.

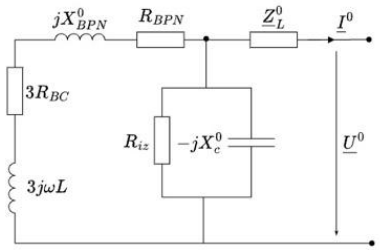

Fig. 2. Zero-sequence equivalent circuit of the substation and the medium voltage electrical network

The positive-sequence equivalent electrical circuit of the medium voltage network is presented in Fig. 3, where the following notation conventions are used: $\underline{Z}^+_{Tr.1}$ – positive-sequence impedance of the transformer Tr. 1; $\underline{Z}^+_{BPN}$ – positive-sequence impedance of the zig-zag coil; $\underline{Z}^+_{Le}$ – positive-sequence equivalent impedance of the lines without fault; $\underline{Z}^+_L$ – positive-sequence impedance of the faulted line from the busbar to the fault location; $\underline{Z}^+_s$ – positive-sequence impedance of the loads; $\underline{U}^+$ – positive-sequence voltage at the fault location; $\underline{U}_f$ – phase-voltage at the fault location before fault occurrence; $\underline{I}^+$ – positive-sequence current at the fault location.

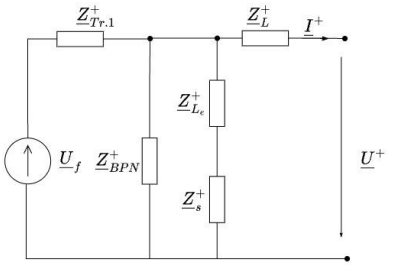

Fig. 3. Positive-sequence equivalent circuit of the substation and the medium voltage electrical network

The negative-sequence equivalent electrical circuit of the medium voltage network is presented in Fig. 4, where the following notation conventions are used: $\underline{Z}^-_{Tr.1}$ – negative-sequence impedance of the transformer Tr. 1; $\underline{Z}^-_{BPN}$ – negative-sequence impedance of the zig-zag coil; $\underline{Z}^-_{Le}$ – negative-sequence equivalent impedance of the lines without fault; $\underline{Z}^-_L$ – negative-sequence impedance of the faulted line from the busbar to the fault location; $\underline{Z}^-_s$ – positive-sequence impedance of the loads; $\underline{U}^-$ – negative-sequence voltage at the fault location; $\underline{I}^-$ – negative-sequence current at the fault location.

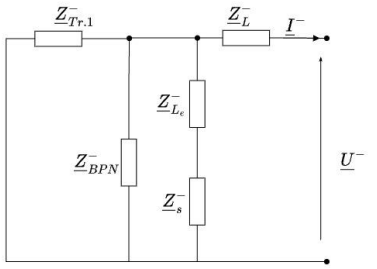

Fig. 4. Negative-sequence equivalent circuit of the substation and the medium voltage electrical network

In case of a single line-to-ground fault, these equivalent circuits are connected in series, therefore the sequence currents are computed using (1)

$$\underline{I}^0=\underline{I}^+=\underline{I}^-=\frac{U_f}{\underline{Z}^++\underline{Z}^-+\underline{Z}^0+3R_t} \tag{1}$$

whereas the zero-sequence voltage of the substation busbars using (2)

$$\underline{U}^0=-\underline{Z}^0\underline{I}^0 \tag{2}$$

measurements based on which the protective relays make a discriminatory decision. In (1) and (2), the zero-sequence impedance from the fault location, $\underline{Z}^0$ (Fig. 2), is expressed using (3)

$$\underline{Z}^0=Z_L^0+\frac{\left[R_{BPN}+3R_{BC}+j\left(X_{BPN}^0+3\omega L\right)\right]\frac{R_{iz}\left(-jX_c^0\right)}{R_{iz}-jX_C^0}}{R_{BPN}+3R_{BC}+j\left(X_{BPN}^0+3\omega L\right)} \tag{3}$$

Assuming the current resonance condition for the circuit in Fig. 2 is fulfilled, if the insulation is perfect, the inductance L of the Petersen coil is computed using (4).

$$L=\frac{1}{3\omega}\left[\frac{X_C^0+\sqrt{\left(X_C^0\right)^2-4\left(R_{BPN}+3R_{BC}\right)^2}}{2}-X_{BPN}\right] \tag{4}$$

From Fig. 5 a value of L equal to 0.811 H is chosen.

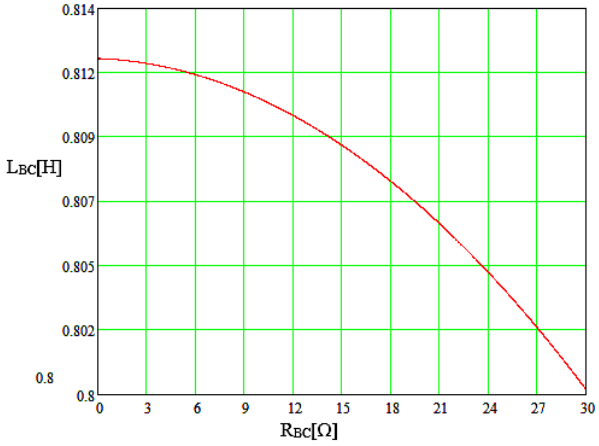

Fig. 5. Petersen coil inductance L_{BC} as a function of coil electrical resistance R_{BC}, network at resonance

If the neutral physical point of the medium voltage network is grounded via an arc-suppression coil, the consumers supplied by the medium voltage lines are not affected during a single line-to-ground fault and, therefore, it is not necessary to disconnect them from the power source. Provided the Petersen coil is properly tuned, more than 80% of single line-to-ground faults are eliminated without the need to disconnect the faulty line from the power source. As in the case of isolated neutral networks, in resonant grounding distribution networks, if the single line-to-ground fault is not removed, it can turn into a double line-to-ground fault or even a three-phase fault. To avoid such situations, it is necessary that the medium voltage electrical networks are equipped with both sensitive and selective protection devices that ensure the detection of the fault in the shortest time possible. Detecting single line-to-ground faults in their early stages, when the electrical resistance at the fault location is high, prevents the occurrence of multiple faults. Various methods of selective single line-to-ground fault detection are proposed in [3], [7], [9], [12], [14], [16], [17], [29], [30], [31]. For the proper design of these protection schemes, accurate mathematical models that consider the evolution of both the voltages and the currents in the medium voltage network during fault are needed.

The real 20 kV electrical network from Fig. 1 is considered for the analysis of a single line-to-ground fault on the line L_1, given that the experimental results during such a fault are available. The following notation conventions are used: K – fault location; R_t – fault resistance; Tr. 1 – 110/20 kV transformer (nominal apparent power 16 MVA, wye with ground (Y_0) connection on the 110 kV side and delta (Δ) on the 20 kV side); L_1 – Faulted line; L_2 – Line without fault having capacitive current I_{ca} 1,84 A, I_{cr} 6,86 A, and loss angle $\delta = 15°$; L_3 – Line without fault having capacitive current I_{ca} 0,705 A, I_{cr} 20,19 A, and loss angle $\delta = 2°$, and L_4 - Line without fault having capacitive current I_{ca} 1,95 A, I_{cr} 20,21 A, and loss angle $\delta = 5,5°$. The network total capacitive current was experimentally measured at I_{ca} 4,49 A and I_{cr} 47,26 A, whereas the loss angle $\delta = 5,43°$. For the 20 kV line voltage, the phase voltage is equal to 11,547 kV. The fault current and the zero-sequence voltage of the medium voltage busbars are measured. The values of the parameters of the electrical equipments from Fig. 1 are given in TABLE I. , TABLE II. and TABLE III.

TABLE I. SEQUENCE IMPEDANCES OF THE ELEMENTS FROM FIG. 1

Electrical equipment	**Sequence impedances**		
	positive	***negative***	***zero***
Tr. 110kV/20kV	0,61+j2,75	0,61+j2,75	∞
Zig-zag coil	2,78+j697,4	2,78+j697,4	2,78+j8,34
20 kV lines [Ω/km]	25,59+j11,91	25,59+j9,53	∞
Loads (accounting for 91% of transformer power. at 0,9 power factor)	25,59+j11,91	25,59+j9,53	∞

TABLE II. PARAMETERS OF THE 20 KV LINES WITHOUT FAULT

Line	**Loss angle [°]**	**Capacitive current [A]**		$\mathbf{R_{iz}}$ **[Ω]**	$\mathbf{X_C^0}$ **[Ω]**
		I_{ca}	I_{cr}		
L2	15	1,84	6,86	19891	5335,3
L3	2	0,705	20,19	51915	1812,8
L4	5,5	1,95	20,21	19769	1811
Network	5,43	4,49	47,26	8151,4	774,44

TABLE III. THE PETERSEN COIL OPERATING REGIMES

Network operating at	$\mathbf{Z_{BC}}$ **[Ω]**	**Argument** $\mathbf{Z_{BC}}$ **[°]**	$\mathbf{R_{BC}}$ **[Ω]**	$\mathbf{X_L}$ **[Ω]**
Undercompensation 4,5%	267,46	87	14	267,1
Overcompensation 6,1%	239,53	83	29,2	237,7
Undercompensation 36,9%	406,61	89	7,1	406,5
Resonance	255,21	87	13,36	254,9

For this network, experimental results during a single line-to-ground fault are available (TABLE IV.), therefore, the results yielded by the analytical models (one considering ideal elements, $R_{BC}=0$ and $R_{iz}=\infty$, and one considering real elements, R_{BC} from TABLE III. and $R_{iz}=8151,4\ \Omega$) could be compared against these (i.e., the results for the network operating at 4,5% undercompensation are tabulated in TABLE V.).

TABLE IV. EXPERIMENTAL VALUES DURING SINGLE LINE-TO-GROUND FAULT (ZERO-SEQUENCE VOLTAGE AS REFERENCE)

Network operating at	$\mathbf{R_t}$ **[Ω]**	$\mathbf{I_d}$ **[A]**	$\mathbf{3\underline{I}_2^0}$ **[A]**	$\mathbf{3\underline{I}_3^0}$ **[A]**	$\mathbf{3\underline{I}_4^0}$ **[A]**	$\mathbf{I_{BC}}$ **[A]**
Undercompensation 4,5%	8	$7,8e^{j102°}$	$7,1e^{j75°}$	$20,2e^{j88°}$	$20,3e^{j84°}$	$45,8e^{-j87°}$
	268	$5,8e^{j107°}$	$6,8e^{j109°}$	$20,3e^{j93°}$	$18,9e^{j84,5°}$	$44,1e^{-j89°}$
Overcompensation 6,1%	8	$12,7e^{j100°}$	$6,5e^{j75°}$	$20,8e^{j88°}$	$20,4e^{j84,5°}$	$52,3e^{-j83°}$
	268	$11,8e^{j94°}$	$6,2e^{j75°}$	$21,2e^{j88°}$	$18,5e^{j84,5°}$	$49,3e^{-j83°}$
Undercompensation 36,9%	8	$7e^{-j96°}$	$6,5e^{j75°}$	$20,8e^{j88°}$	$20,3e^{j84,5°}$	$33,1e^{-j89°}$
	268	$7,1e^{-j102°}$	$7e^{j75°}$	$20,1e^{j88°}$	$19e^{j84,5°}$	$32,3e^{-j89°}$

TABLE V. ANALYTICAL MODEL VALIDATION, RESONANT GROUNDING, I.E., UNDERCOMPENSATION 4,5%

Rt [Ω]					**Error [%]**		
		Analytical		**Experimental**	$\boldsymbol{\varepsilon_1}$	$\boldsymbol{\varepsilon_2}$	$\boldsymbol{\varepsilon_3}$
		Ideal ($R_{BC}=0$ and $R_{iz}=\infty$)	**Real (R_{BC} from TABLE III. and $R_{iz}=8151,4\ \Omega$)**				
8	U^0 [V]	12530	12470	12200	-2,21	0,48	2,63
	I^0 [A]	0,726	2,494	2,406	-3,66	70,9	69,8
268	U^0 [V]	12480	10850	11920	8,98	13,06	4,49
	I^0 [A]	0,723	2,17	2,011	-7,91	66,7	64,1

The errors from TABLE V. are computed using (5):

$$\varepsilon_1[\%]=\frac{\text{real value-experimental value}}{\text{experimental value}}100$$

$$\varepsilon_2[\%]=\frac{\text{real value-ideal value}}{\text{experimental value}}100 \quad (5)$$

$$\varepsilon_3[\%]=\frac{\text{experimental value-ideal value}}{\text{experimental value}}100$$

Regardless of the network operating regime, considering that the network parameters values from the analytical model may vary slightly from the actual ones, the errors are admissible. However, the setting of the protective relays must be reviewed periodically and updated according to the latest parameters values determined experimentally, because these change over time due to either common phenomena, such as ageing, histeresis or eddy-currents, or power quality issues, i.e., non-sinusoidal supply voltages or currents flowing through the Petersen coil. The cumulative influence of both the insulation resistance (Fig. 6, for R_{BC}=13,36 Ω, and Fig. 7, for R_{BC}=0 Ω) and the coil resistance (Fig. 8, R_{iz}=8151,4 Ω, and Fig. 9, R_{iz}=∞) for a given fault resistance on the zero-sequence values of the voltage and the current are shown in Fig. 10 and Fig. 11 for the network with resonant grounding operating at resonance.

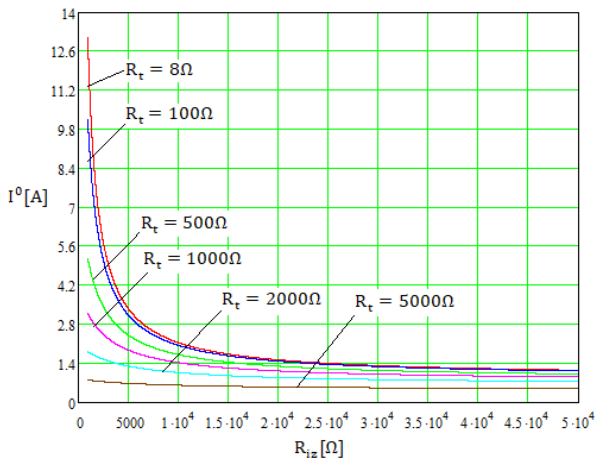

Fig. 6. The influence of the insulation resistance on the zero-sequence current, network operating at resonance, R_{BC}=13,36 Ω

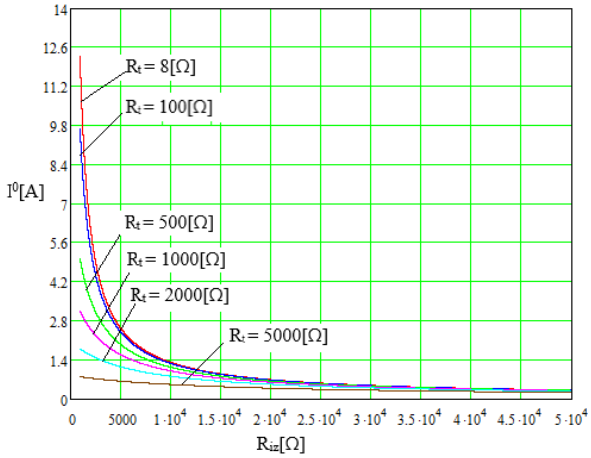

Fig. 7. The influence of the insulation resistance on the zero-sequence current, network operating at resonance, R_{BC}=0

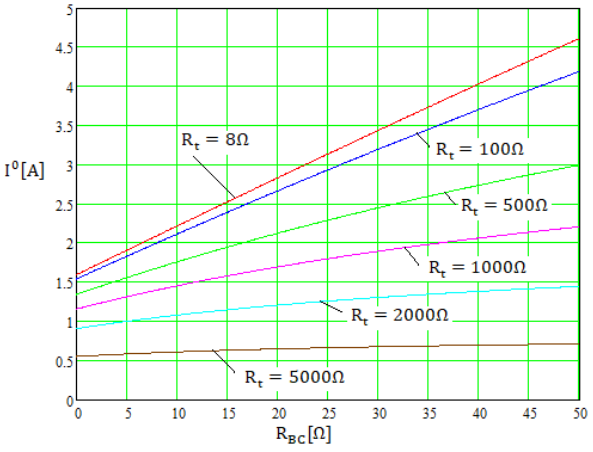

Fig. 8. The influence of the coil resistance on the zero-sequence current, network operating at resonance, R_{iz}=8151,4 Ω

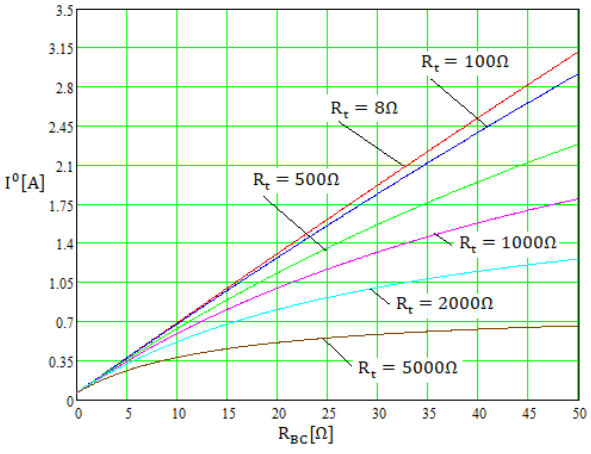

Fig. 9. The influence of the coil resistance on the zero-sequence current, network operating at resonance, R_{iz}=∞

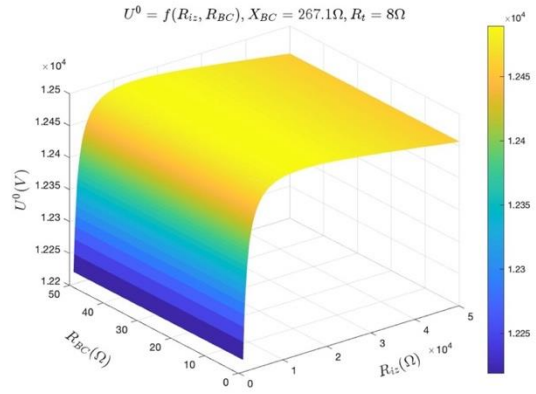

Fig. 10. The cumulative influence of both the insulation resistance and the coil resistance on the zero-sequence voltage, network operating at resonance

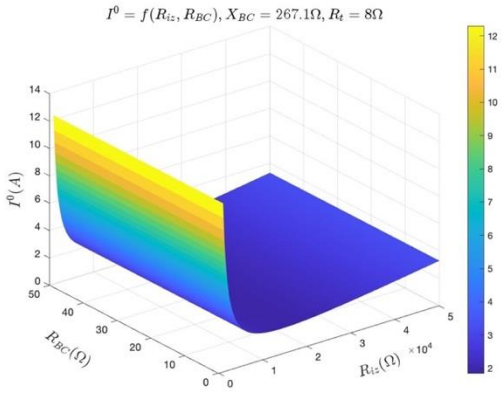

Fig. 11. The cumulative influence of both the insulation resistance and the coil resistance on the zero-sequence current, network operating at resonance

3. MATLAB/SIMULINK ENVIRONMENT

Given the wide diversity in design and operation of the distribution feeders, a practical modelling methodology using software tools would provide energy planners and technical practitioners with an overview of key issues and concerns around long-term scenario planning. The practical modelling methodology introduced in [24] and the workflow from [32] is applied to model the networks from Fig. 1 and Fig. 12 in the MATLAB/Simulink environment. In the case of the blocks used in MATLAB/Simulink, each of them was introduced before 2006, peer reviewed and used in numerous applications ever since.

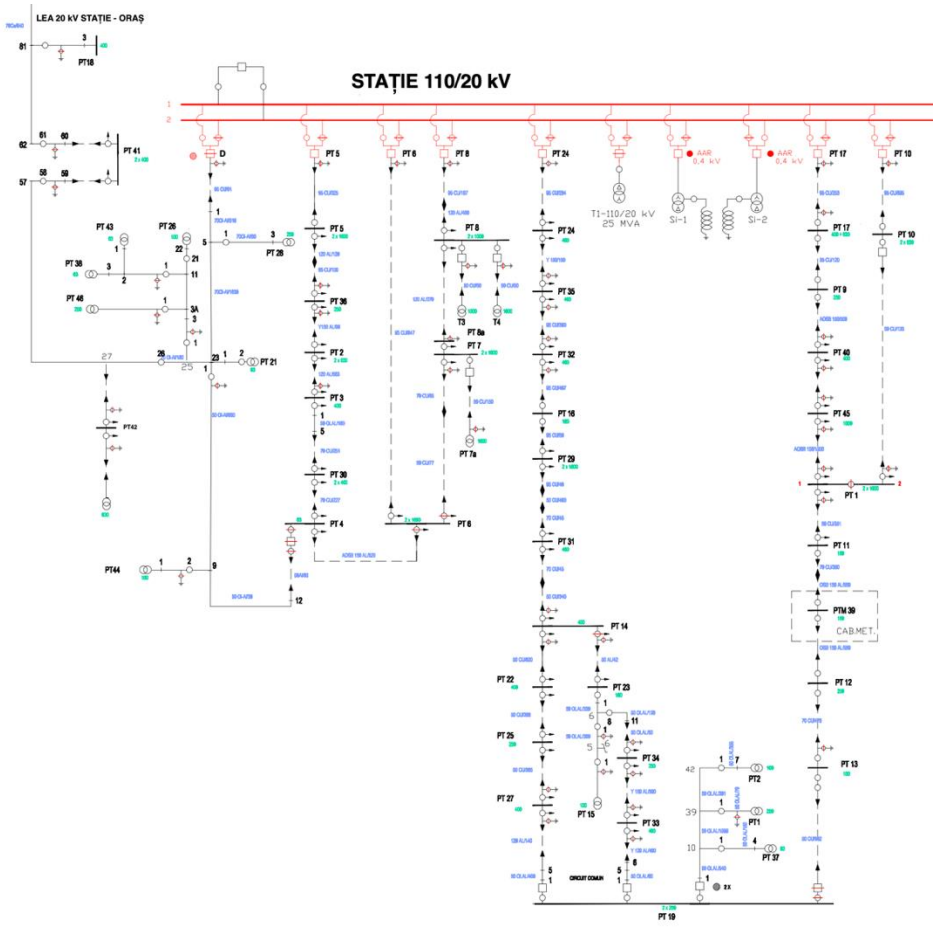

Fig. 12. Single line diagram of a section from a real distribution network

The 110 kV distribution network is modelled as a three-phase voltage source with a RL branch in series. Its short-circuit level parameters values are computed according to IEC 60076-5 [33] for the electrical characteristics of the 110 kV/20 kV voltage transformer, which are the X/R ratio and the base voltage, X and R being the total reactance and resistance (network plus transformer) reactance and resistance, respectively. A three-phase transformer block with two windings and configurable winding connection is used for the HV/MV transformer. The system neutral physical point is provided by the zigzag winding connection of the artificial neutral coil created using three mutual inductances with two windings and an equal mutual term. Because of the opposite winding polarities, the coil offers a very high impedance under normal conditions. Under fault conditions, only the zero-sequence current flows through the six upper and lower windings. Should the coil be supplied with positive- and zero-sequence voltages, respectively, then the corresponding positive- and zero-sequence currents flow through it, the latter being 132,9 times higher than the former, thus fulfilling a criterion used to validate the model functionality (Fig. 13). The Petersen coil is modelled as a RL series branch. Both overhead lines and underground cables from Fig. 12 are modelled as PI section lines with lumped parameters consisting of a RL series branch and two shunt capacitances at both ends. However, for the network from Fig. 1 only the transverse parameters of the healthy lines, i.e., the phase-to-earth capacitance of the phase conductors and the electrical resistance corresponding to the insulation active power losses, are considered, modelled using two series R-L-C branches of type R and C, respectively, conected in parallel. The loads are either derived from the customer demand curves or computed as a percentage from the transformer power at a given power factor, and are modelled as constant real and reactive power wye connected three-phase series RLC load, R being the resistance, L the inductance, and C the capacitance.

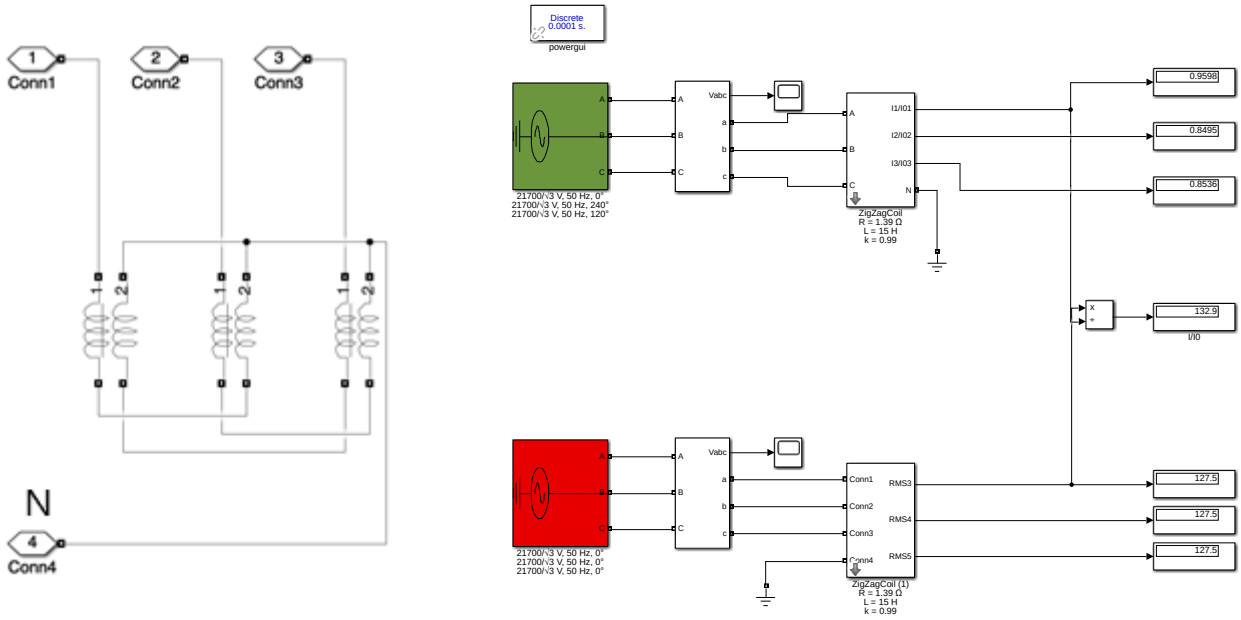

Fig. 13. Zig-zag coil MATLAB/Simulink model validation

Moreover, a library comprised of built-in and user-defined blocks and subsystems that are necessary for: different high impedance fault conditions simulation, symmetrical component measurements, signal processing, feature extraction, and assessment of relay operation is also introduced (TABLE VI.). The custom blocks are created using the built-in ones connected appropriately in a masked subsystem. The mask is used to initialise and to input parameters values.

TABLE VI. LIBRARY SUMMARY

Class	Description
Symmetrical components filters	Instrument transformers for scaling down the input quantity to the accuracy expected for a particular measurement (voltage, current).
Signal processing	Functions used for preprocessing the input signal in discrete time.
Feature extraction	Functions used for analysing the input signal in both the discrete time and frequency domains.
Relays	Protection devices that operate when their input exceeds the predetermined values.
Fault models	Computational models of the electric arc for fault scenario simulation.

Regarding the comparison of the experimental values against the simulation results, and thus the assessment of accuracy of the model from Fig. 14, for the network operating at 4,5% undercompensation, TABLE VII. highlights the influence of the total capacitive reactance on the zero-sequence values, especially the currents, where the errors range from 27,01 to -5,29%, if this reactance varies 1% at a time, from 100% to 90%.

TABLE VII. THE INFLUENCE OF THE TOTAL CAPACITIVE REACTANCE ON THE ZERO-SEQUENCE VOLTAGE AND CURRENT VALUES, NETWORK AT 4,5% UNDERCOMPENSAION, FAULT RESISTANCE 8 OHMS

k	**1**	**0,99**	**0,98**	**0,97**	**0,96**	**0,95**	**0,94**	**0,93**	**0,92**	**0,91**	**0,90**
kX_C^0 [Ω]	774,44	766,70	758,95	751,21	743,46	735,72	727,97	720,23	712,48	704,74	697,00
I^0 [A]	3,056	2,944	2,837	2,737	2,645	2,559	2,483	2,416	2,359	2,313	2,279
ε_I [%]	27,01%	22,35%	17,93%	13,78%	9,91%	6,38%	3,20%	0,41%	-1,95%	-3,86%	-5,29%
U^0 [V]	12234,45	12232,86	12231,26	12229,67	12228,08	12226,48	12224,89	12223,29	12221,70	12220,10	12218,51
ε_U [%]	0,28%	0,27%	0,26%	0,24%	0,23%	0,22%	0,20%	0,19%	0,18%	0,16%	0,15%

The error ε from the table is computed using (6):

$$\varepsilon[\%]=\frac{\text{experimental value-simulation value}}{\text{experimental value}}100 \tag{6}$$

The numerical model is therefore considered precise enough for the further analysis of the transient regime caused by a single line-to-ground fault in the network from Fig. 1, which, it should be also emphasized, would otherwise be a very challenging analytical task.

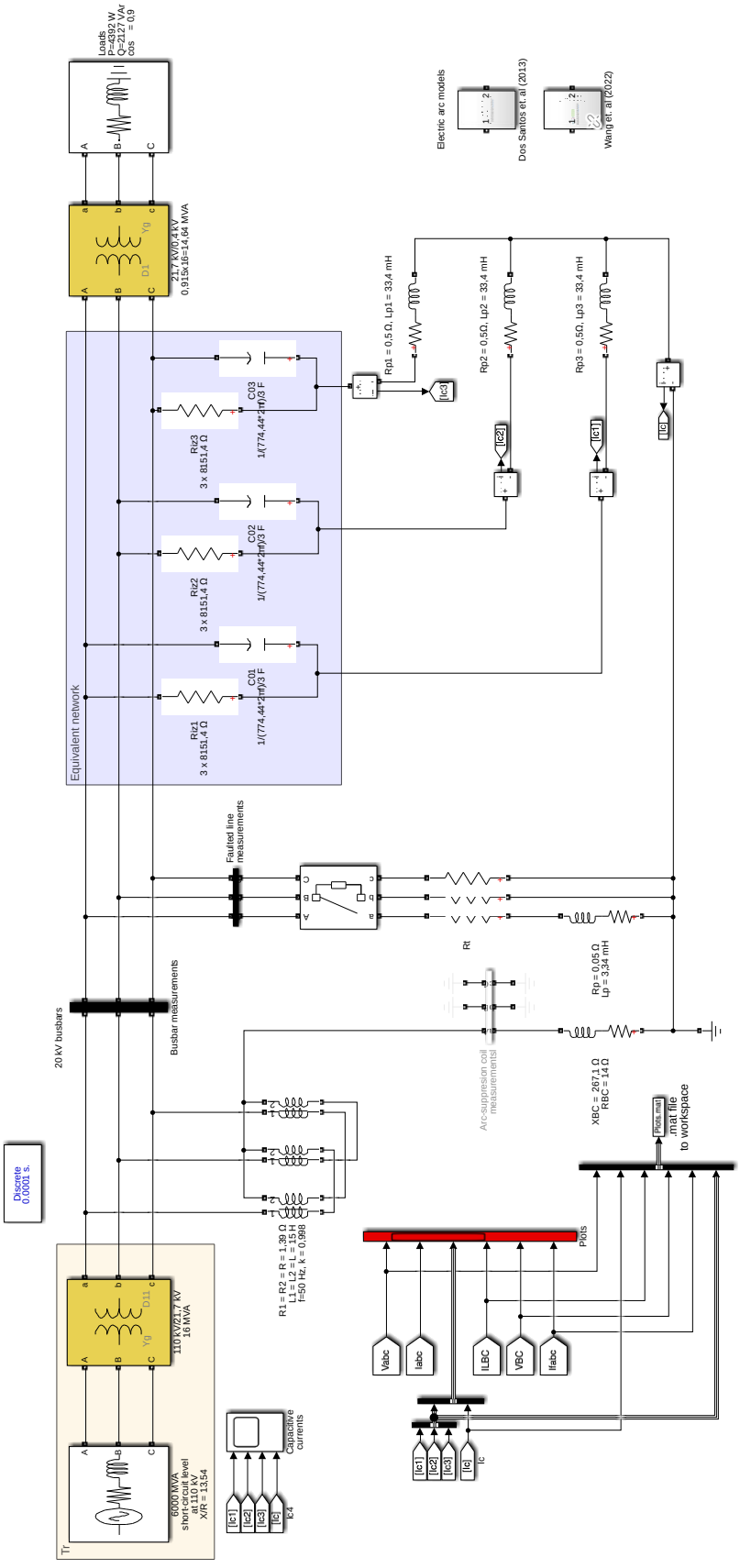

Fig. 14. Simulink model of the network from Fig. 1

4. ANALYSIS OF THE TRANSIENT REGIME CAUSED BY A SINGLE LINE-TO-GROUND FAULT IN A THREE-PHASE ELECTRICAL INSTALLATIONS

Simulations were conducted for both the operating regimes from TABLE III. andTABLE III. TABLE IV. and for the hypothetical cases of resistor and isolated grounding It is assumed that the single line-to-ground fault occurs on feeder L_1, on substation busbars. The fault resistance is 8 ohms (and 268 ohms for resonance only). Firstly, the initial phase of the faulted line is varied in order to pinpoint the maximum value of the fault current during transients (Fig. 15). Secondly, the influence of the grounding method is analysed (Fig. 16). Thirdly, the state of the insulation is first modelled as perfect, the loss angle δ being equal to 0°, then as imperfect, the loss angle δ being equal to 5,43°. The values corresponding to an imperfect insulation (loss angle equal to 5,43°) are compared against the values corresponding to a perfect insulation (loss angle equal to 0°) for all of the network operating regimes (Fig. 17). Lastly, two arc models are considered to highlight the features of the signals measured during such faults: low fault current, long duration, waveform distortion, asymmetry, time-varying current amplitude during fault (build-up, shoulders), intermittence and randomness (Fig. 18). The data from simulation are written into a defined variable Measurements from the .mat file, which is an array containing the busbar phase voltages and currents in the subsequent rows. Using the MATLAB Live Editor feature for user-defined functions, the zero-sequence busbar voltage and the fault current are then computed after the damping of the transient regime and their RMS values are stored in an Excel file together with the transients duration (i.e. TABLE VIII. for resonance).

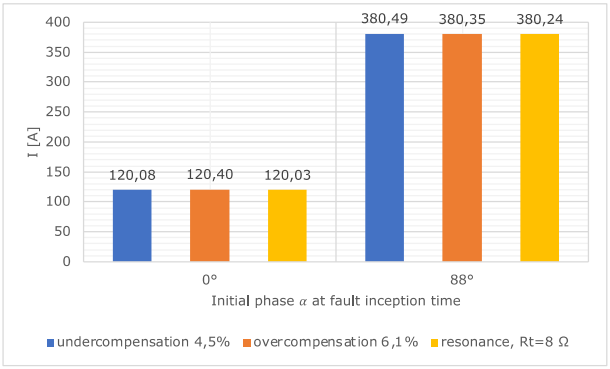

a)

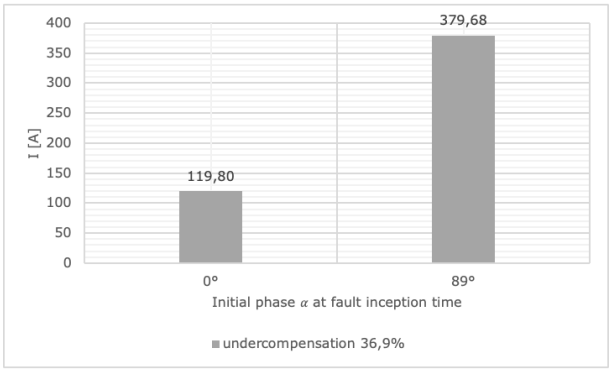

b)

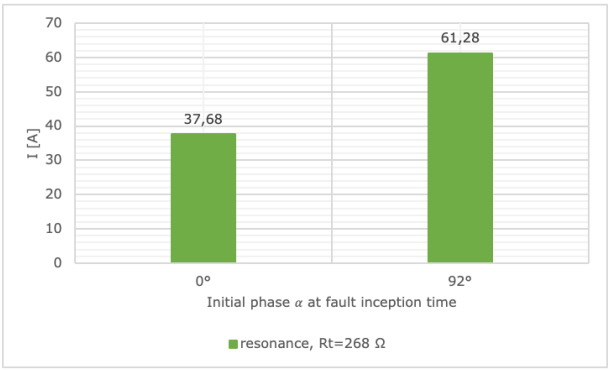

c)

Fig. 15. Fault current values at initial phase α=0° and at α coresponding to the maximum value, R_t=8 Ω

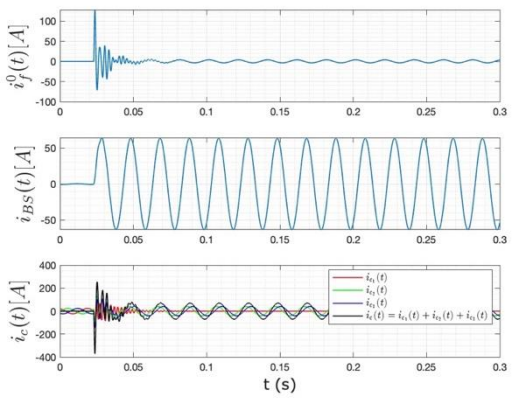

a) Resonant grounding, at resonance

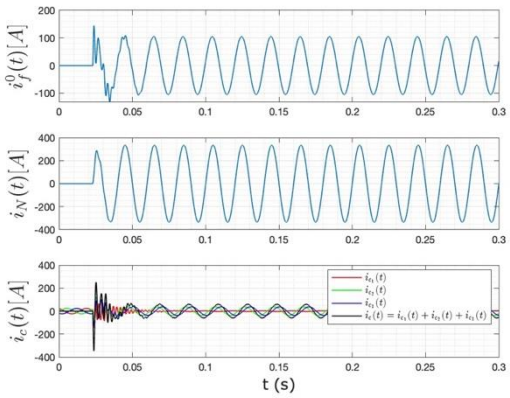

b) Resistance grounding network, R_N=37,5 Ω

Fig. 16. Time variation during a single line-to-ground fault, α=90°, R_f=8 Ω,
of: $i_f^0(t)$ – zero-sequence current faulted line; $i_{BS}(t)$ – Petersen coil current; $i_{c_1}(t)$, $i_{c_2}(t)$, $i_{c_3}(t)$, $i_c(t) = i_{c_1}(t) + i_{c_2}(t) + i_{c_3}(t)$ – capacitive currents

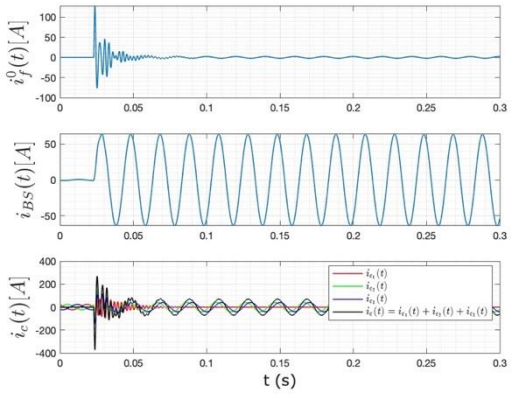

a) R_{iz}=∞

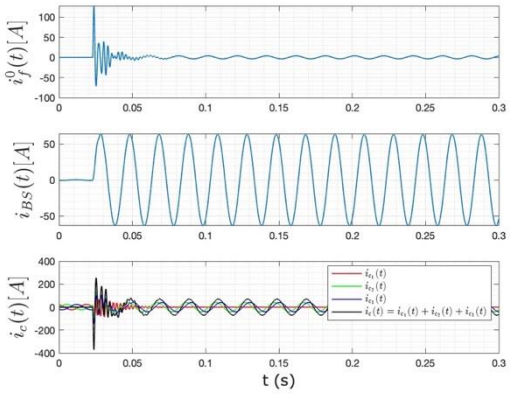

b) R_{iz}=8151,4 Ω

Fig. 17. Time variation during a single line-to-ground fault, network at resonance, α=90°, R_f=8 Ω,
of: $i_f^0(t)$ – zero-sequence current faulted line; $i_{BS}(t)$ – Petersen coil current; $i_{c_1}(t)$, $i_{c_2}(t)$, $i_{c_3}(t)$, $i_c(t) = i_{c_1}(t) + i_{c_2}(t) + i_{c_3}(t)$ – capacitive currents

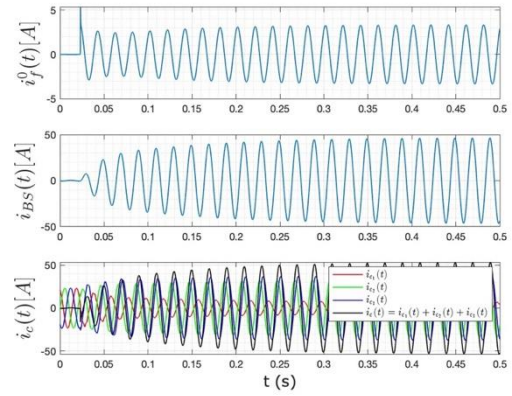

a) Arc fault [34]

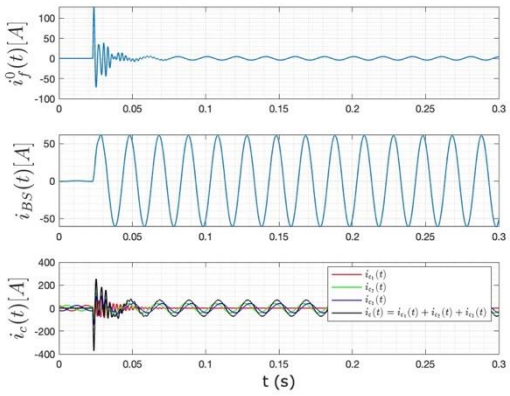

b) R_f=8 Ω

Fig. 18. Time variation during a single line-to-ground fault, undercompensation 4,5%,
of: $i_f^0(t)$ – zero-sequence current faulted line; $i_{BS}(t)$ – Petersen coil current; $i_{c_1}(t)$, $i_{c_2}(t)$, $i_{c_3}(t)$, $i_c(t) = i_{c_1}(t) + i_{c_2}(t) + i_{c_3}(t)$ – capacitive currents

TABLE VIII. SIMULATION RESULTS FOR A SINGLE LINE-TO-GROUND FAULT, NETWORK OPERATING AT RESONANCE, FAULT RESISTANCE 8 OHMS

R_t – fault resistance; α – initial phase of the faulted line; R_{iz} – insulation resistance; t_0 – fault inception angle; t_1 – fault transients end time, during $[t_0, t_1]$ the zero-sequence current is measured; Δt – transients duration; T – period after the damping of the transient regime (20 ms for 50 Hz); $\Delta t/T$ – transients duration in periods; U_{1max}, U_{2max}, U_{3max} – busbar voltages maximum values during transients; U^0_{max} – zero-sequence maximum voltage value; I^0_{fmax} – zero-sequence current maximum value; I_{BSmax} – Petersen coil current maximum value; I_{fmax} – fault current maximum value; U_{1ef}, U_{2ef}, U_{3ef} – phase-voltages RMS values; U^0_{ef} – zero-sequence voltage RMS value; I^0_{fef} – zero-sequence current RMS value; I_{BSef} – Petersen coil current RMS value; inf – $R_{iz}=\infty$.

R_t [Ω]	8	8	8	8	8	8	8	8	8	8	8
α [°]	0	15	88	89	90	91	92	0	90	91	92
R_{iz} [Ω]	8151,4	8151,4	8151,4	8151,4	8151,4	8151,4	8151,4	inf	inf	inf	inf
t_0 [s]	0,0180	0,0188	0,023	0,023	0,0230	0,0231	0,0231	0,0180	0,0230	0,0231	0,0231
t_1 [s]	0,236	0,236	0,117	0,117	0,107	0,107	0,107	0,445	0,125	0,125	0,125
Δt [s]	0,2180	0,2172	0,094	0,094	0,0840	0,0839	0,0839	0,4270	0,1020	0,1019	0,1019
$\Delta t/T$	10,90	10,86	4,71	4,70	4,20	4,20	4,19	21,35	5,10	5,10	5,09
U_{1max} [V]	1118,64	1326,03	4200,78	4204,70	17560,55	4204,47	4200,09	1113,23	17717,40	4234,61	4229,27
U_{2max} [V]	31063,00	31064,20	31528,77	31354,28	31162,95	31162,95	30957,02	31270,38	31465,63	31465,63	31239,86
U_{3max} [V]	21657,04	21681,47	22055,09	22052,86	22076,84	22088,58	22084,57	21688,80	21897,94	21907,54	21903,92
U^0_{max} [V]	17935,02	17926,43	18592,25	18687,84	18765,36	18765,36	18824,35	18099,23	19087,10	19087,10	19143,09
I^0_{fmax} [A]	40,01	46,15	126,75	126,65	126,53	126,53	126,29	39,71	127,26	127,26	126,99
I_{BSmax} [A]	112,28	111,80	68,14	66,29	64,42	64,42	63,08	120,96	67,54	67,54	65,49
I_{fmax} [A]	120,03	138,45	380,24	379,9	379,60	379,60	378,88	119,12	381,79	381,79	380,98
U_{1ef} [V]	66,10	66,10	66,67	66,63	66,58	66,58	66,63	35,19	34,57	34,57	34,44
U_{2ef} [V]	21284,02	21284,02	21569,77	21569,80	21573,17	21573,17	21573,13	21144,34	21522,98	21522,98	21522,84
U_{3ef} [V]	21535,30	21535,30	21600,75	21600,77	21605,51	21605,51	21605,49	21732,01	21730,32	21730,32	21730,30
U^0_{ef} [V]	12188,21	12188,22	12392,53	12392,57	12397,27	12397,27	12397,23	12222,87	12440,12	12440,12	12440,03
I^0_{fef} [A]	2,70	2,70	2,73	2,73	2,73	2,73	2,73	1,44	1,42	1,42	1,41
I_{BSef} [A]	45,86	45,86	45,14	45,14	45,13	45,13	45,13	46,20	45,42	45,42	45,40
I_{fef} [A]	8,09	8,09	8,19	8,18	8,18	8,18	8,18	4,31	4,25	4,25	4,23

5. CONCLUSIONS

In a medium voltage network with resonant grounding, neglecting the insulation active power losses when the fault current and the medium voltage zero-sequence busbars voltage are computed leads to erroneous results. The errors depend on the network operating regime and on the fault resistance value. The highest errors are obtained when the medium voltage network operates at resonance. In this case, the values of the fault current and the zero-sequence busbars voltage are strongly influenced by the state of the insulation. It is for this reason that the setting of the protective relays used to detect single line-to-ground faults must be reviewed periodically and updated according to the latest insulation strength parameters values. If the medium voltage network operates at overcompensation, the influence of the insulation active power losses on the fault current and on the zero-sequence busbars voltage is mitigated. However, by tuning the coil away from resonance, its efficiency in extinguishing the electric arc during a single line-to-ground fault is decreased, i.e., the number of self-clearing single line-to-ground faults (faults that are removed without disconnecting the faulty line from the source) are reduced. Moreover, the electrical resistance of the Petersen coil depends on the electrical resistance of the winding and the active power losses in the coil ferromagnetic core. The non-sinusoidal variation of the current through the coil leads to an increase of the active power losses in the ferromagnetic core, and thus to an increase of the electrical resistance. Regardless of the operating regime, higher fault resistance values damp the transient components of voltage and fault current, thus the transient regime is shorter and less dangerous. This thesis provides researchers and technical practitioners with an overview of the influence of the medium voltage distribution network parameters on the measurements based on which the protective relays make a discriminatory decision should a single line-to-ground fault occur. It emphasized the importance of the accurate representation of

the electrical network with imperfect insulation, and the deployment of the presented model instead of the canonical one used in the network design stage, which does not resemble the contingencies present in distribution networks during faults accurately.

REFERENCES

[1] C. S. Mardegan and R. Rifaat, 'Insights into applications of IEEE Standards for Ground Fault Protection in Industrial and Commercial Power Systems', in *2014 IEEE/IAS 50th Industrial & Commercial Power Systems Technical Conference*, May 2014, pp. 1–10. doi: 10.1109/ICPS.2014.6839181.

[2] A. K. Abbas, S. Hamad, and N. A. Hamad, 'Single line to ground fault detection and location in medium voltage distribution system network based on neural network', *Indones. J. Electr. Eng. Comput. Sci.*, vol. 23, no. 2, Art. no. 2, Aug. 2021, doi: 10.11591/ijeecs.v23.i2.pp621-632.

[3] A. Ukrainicev, V. Nagy, I. Nagy, S. Sarry, and G. Chmihaloy, 'Analysis of the functioning of the earth fault protection with active influence on electrical grid', presented at the Proceedings of the 9th International Scientific Symposium on Electrical Power Engineering, Stará Lesná, Slovakia, Sep. 2017, pp. 418–421.

[4] J. Ma, X. Yan, B. Fan, C. Liu, and J. S. Thorp, 'A Novel Line Protection Scheme for a Single Phase-to-Ground Fault Based on Voltage Phase Comparison', *IEEE Trans. Power Deliv.*, vol. 31, no. 5, pp. 2018–2027, Oct. 2016, doi: 10.1109/TPWRD.2015.2507600.

[5] X. Zhang, B. Xu, Z. Pan, and P. Wei, 'Study on single-phase earthed faulty feeder selection methods in non-solidly grounded systems', in *2008 Third International Conference on Electric Utility Deregulation and Restructuring and Power Technologies*, Apr. 2008, pp. 1836–1840. doi: 10.1109/DRPT.2008.4523705.

[6] D. Toader, S. Haragus, and C. Blaj, 'Numeric simulation of faults in electrical networks', presented at the Proceedings of the 10th WSEAS International Conference on Fuzzy Systems, Prague, Czech Republic, Mar. 2009.

[7] Z. Liu and C. Deng, 'SINGLE-PHASE GROUND FAULT LINE SELECTION METHOD IN ACTIVE DISTRIBUTION NETWORKS BASED ON HIGH-VOLTAGE INVERTER INJECTED SIGNALS', *DYNA*, vol. 94, no. 1, pp. 539–545, Sep. 2019, doi: 10.6036/9221.

[8] D. Toader, C. Blaj, P. Ruset, I. D. Hategan, N. Pinte, and B. Arvinti, 'Device for Automatic Control of the Petersen Coil', in *Soft Computing Applications*, V. E. Balas, L. C. Jain, and B. Kovačević, Eds., in Advances in Intelligent Systems and Computing. Cham: Springer International Publishing, 2016, pp. 1121–1137. doi: 10.1007/978-3-319-18416-6_91.

[9] D. Toader, P. Ruset, I. Hategan, I. Diaconu, and N. Pinte, 'Selective detection of simple and doublegrounding within the medium voltage electrical networks with compensated null', in *2009 IEEE Bucharest PowerTech*, Jun. 2009, pp. 1–9. doi: 10.1109/PTC.2009.5281893.

[10] Y. Gao, X. Lin, P. Liu, and Z. Bo, 'A Generalized Morphological Transform Based Faulty Feeder Selector Suitable for the Non-Effectively Grounded Power Systems', in *2007 IEEE Power Engineering Society General Meeting*, Jun. 2007, pp. 1–6. doi: 10.1109/PES.2007.385772.

[11] J. Li, G. Wang, D. Zeng, and H. Li, 'High-impedance ground faulted line-section location method for a resonant grounding system based on the zero-sequence current's declining periodic component', *Int. J. Electr. Power Energy Syst.*, vol. 119, p. 105910, Jul. 2020, doi: 10.1016/j.ijepes.2020.105910.

[12] T. Tang, C. Huang, Z. Li, and X. Yuan, 'Identifying Faulty Feeder for Single-Phase High Impedance Fault in Resonant Grounding Distribution System', *Energies*, vol. 12, no. 4, Art. no. 4, Jan. 2019, doi: 10.3390/en12040598.

[13] B. Fan *et al.*, 'Faulty phase recognition method based on phase-to-ground voltages variation for neutral ungrounded distribution networks', *Electr. Power Syst. Res.*, vol. 190, p. 106848, Jan. 2021, doi: 10.1016/j.epsr.2020.106848.

[14] Z. Li *et al.*, 'Single-phase-to-ground fault section location in flexible resonant grounding distribution networks using soft open points', *Int. J. Electr. Power Energy Syst.*, vol. 122, p. 106198, Nov. 2020, doi: 10.1016/j.ijepes.2020.106198.

[15] Z. Guo, J. Yao, S. Yang, H. Zhang, T. Mao, and T. L. Duong, 'A new method for non-unit protection of power transmission lines based on fault resistance and fault angle reduction', *Int. J. Electr. Power Energy Syst.*, vol. 55, pp. 760–769, Feb. 2014, doi: 10.1016/j.ijepes.2013.10.027.

[16] Z. Pang *et al.*, 'A Fault Section Location Method Based on Energy Remainder of Generalized S-Transform for Single-phase Ground Fault of Distribution Networks', in *2018 IEEE 3rd Advanced Information Technology, Electronic and Automation Control Conference (IAEAC)*, Oct. 2018, pp. 1511–1515. doi: 10.1109/IAEAC.2018.8577513.

[17] J. Meng, W. Wang, X. Tang, and X. Xu, 'Zero-sequence voltage trajectory analysis for unbalanced distribution networks on single-line-to-ground fault condition', *Electr. Power Syst. Res.*, vol. 161, pp. 17–25, Aug. 2018, doi: 10.1016/j.epsr.2018.03.024.

[18] D. Toader, C. Blaj, S. Haragus, I. Cata, and I. Hategan, 'PSpice simulation of single phase in medium voltage electrical networks', presented at the Proceedings of the 3th International Conference on Modern Power Systems, Cluj-Napoca, Romania: Acta Electrotehnica, Special Issue, Oct. 2010, pp. 366–375.

[19] D. Toader, C. Blaj, D. Vesa, I. Tatai, and B. Arvinti, 'Numeric Simulator for the Analysis of Transients due to Fault in Electric Networks', in *2019 8th International Conference on Modern Power Systems (MPS)*, May 2019, pp. 1–6. doi: 10.1109/MPS.2019.8759690.

[20] D. Toader and V. Toaxen, 'Fault transient simulation in distribution networks with improved neutral-point grounding', in *Proceedings of the IASTED International Conference, Power and Energy Systems*, 2000, pp. 125–8.

[21] D. Toader, S. Haragus, C. Blaj, and I. Cata, 'Numerical simulation of single phase faults in medium voltage electrical

networks', vol. 5, pp. 64–74, Jan. 2010.
[22] D. Toader, Ş. Hărăguş, and C. Blaj, 'Virtual system for numeric simulation of three phased circuits. Part 1', in *Proceedings The 7th International Power Systems Conference*, 2007, pp. 22–28.
[23] D. Toader, Ş. Hărăguş, and C. Blaj, 'Virtual system for numeric simulation of three phased circuits. Part 2', in *Proceedings The 7th International Power Systems Conference*, 2007, pp. 29–35.
[24] C. Şolea, D. Toader, M. Vinţan, M. Greconici, D. Vesa, and I. Tatai, 'Framework for distribution network modelling and fault simulation using MATLAB', in *2022 International Conference and Exposition on Electrical And Power Engineering (EPE)*, Oct. 2022, pp. 118–123. doi: 10.1109/EPE56121.2022.9959758.
[25] 'Standard on the insulation choice, insulation coordination and the electrical power devices protection against overvoltages, NTE001/00/03'. 2003.
[26] B. M. Mamikonyan and D. S. Nikoghosyan, 'Measurement of Dielectric Loss by Phase Method', *Am. Sci. Res. J. Eng. Technol. Sci.*, vol. 29, no. 1, pp. 124–137, 2017.
[27] A. P. Mackerras, 'Calculation of Single-Phase Short Circuits by the Method of Symmetrical Components', *Gen. Electr. Rev.*, 1926.
[28] C. L. Fortescue, 'Method of Symmetrical Coordinates Applied to the Solution of Polyphase Networks', *E E TRANS*, 1918.
[29] S.-R. Nam, W.-H. Ko, S. Key, S.-H. Kang, and N.-H. Lee, 'IEC 61850-Based Centralized Protection against Single Line-To-Ground Faults in Ungrounded Distribution Systems', *Energies*, vol. 14, no. 3, p. 722, Jan. 2021, doi: 10.3390/en14030722.
[30] G. Kapoor, 'Wavelet Transform based Detection and Classification of Multilocation Three Phase to Ground Faults in Twelve Phase Transmission Line', 2019.
[31] D. S. Osipov, D. S. Satpaev, and B. Yu. Kisselyov, 'Analysis of Single Phase-to-Ground Fault in Mixed Neutral Ground Systems Using Wavelet Transform', in *2018 International Conference on Industrial Engineering, Applications and Manufacturing (ICIEAM)*, May 2018, pp. 1–5. doi: 10.1109/ICIEAM.2018.8728788.
[32] C. Şolea *et al.*, 'Simultaneous open conductor and ground fault analysis using MATLAB', in *CIGRE Regional South-East European Conference RSEEC 2022 (6th edition)*, Iasi, Romania, Oct. 2022.
[33] 'Power transformers - Part 5: Ability to withstand short circuit'.
[34] W. C. Dos Santos, B. A. De Souza, N. S. D. Brito, F. B. Costa, and M. R. C. Paes, 'High Impedance Faults: From Field Tests to Modeling', *J. Control Autom. Electr. Syst.*, vol. 24, no. 6, pp. 885–896, Dec. 2013, doi: 10.1007/s40313-013-0072-8.